


Article

Investigating the Influencing Factors of Imbibition of Fracturing Fluids in Tight Reservoirs

Jian Liu ¹, Xuefeng Qu ¹, Jiwei Wang ¹, Qiang Liu ¹, Lei Zhang ², Tao Huang ² and Haiyang Yu ^{2,*} 

¹ Research Institute of Exploration and Development, PetroChina Changqing Oilfield Company, Xi'an 710018, China

² State Key Laboratory of Petroleum and Prospecting, China University of Petroleum, Beijing 102249, China

* Correspondence: haiyangyu.cup@139.com

Abstract: Tight reservoirs are the focus of unconventional oil and gas resource development, but most tight reservoirs exhibit complex pore structures, strong non-homogeneity, and limited water drive development. Fracturing fluid imbibition is a critically important way to improve the recovery of tight reservoirs. In this paper, an NMR experimental device was used to conduct imbibition experiments in tight reservoirs, and the relationship between temperature, pressure, matrix permeability, and imbibition recovery was investigated. Based on the fracturing fluid imbibition recovery curve, the imbibition process is divided into the fast imbibition stage, slow imbibition stage, and imbibition equilibrium. In addition, based on the pore structure division, the recovery changes of each pore under different experimental conditions were quantitatively analyzed. The results indicate that the highest imbibition recovery is achieved at an experimental pressure of 5 MPa within the range of 0 MPa to 15 MPa. Increasing the experimental pressure can increase the imbibition rate but will not increase imbibition recovery. Within the investigated range in this paper, fracturing fluid imbibition increases with rising temperature and matrix permeability. Moreover, the recovery of each pore gradually increases with the experimental pressure ranging from 0 MPa to 5 MPa. The recovery of each pore is positively correlated with matrix permeability and temperature. During the experiment, micropores contributed the most to the recovery, while macropores contributed the least. The study in this paper guides the efficient development of tight reservoirs.

Keywords: tight reservoir; fracturing fluids; temperature; pressure; matrix permeability



Citation: Liu, J.; Qu, X.; Wang, J.; Liu, Q.; Zhang, L.; Huang, T.; Yu, H. Investigating the Influencing Factors of Imbibition of Fracturing Fluids in Tight Reservoirs. *Processes* **2024**, *12*, 236. <https://doi.org/10.3390/pr12010236>

Academic Editors: Qibin Li and Carlos Sierra Fernández

Received: 19 December 2023

Revised: 12 January 2024

Accepted: 19 January 2024

Published: 22 January 2024



Copyright: © 2024 by the authors. Licensee MDPI, Basel, Switzerland. This article is an open access article distributed under the terms and conditions of the Creative Commons Attribution (CC BY) license (<https://creativecommons.org/licenses/by/4.0/>).

1. Introduction

Tight oil is an unconventional oil and gas resource characterized by an accumulation origin and occurrence state that differs from conventional oil and gas. Following the commercial exploitation of marine tight oil in North America, tight oil has gained prominence as a focal point in unconventional global exploration and development [1–5]. However, due to the complex genesis and low porosity of reservoirs, the conventional production technology of tight reservoirs faces the challenges of low production of a single well, poor development efficiency, and large-scale application difficulty [6–9].

The large-scale fracturing technology is the key to realizing the efficient development of tight reservoirs. Tight reservoirs are usually produced after a single large-scale volume fracturing, and the depletion development model is adopted in the later stage [10]. The effect of volume fracturing is not only reflected in the hydraulic fracture reconstruction of reservoir rocks within the fracturing construction cycle but also reflected in the hydration imbibition of reservoir rocks in a more extended period so that it can improve the matrix porosity and permeability of the imbibition sweep range of fracturing fluid [11–15]. The minimal radius of the throat in tight reservoirs enhances the capillary imbibition during the whole life cycle of fracturing development, which provides a new method for the synergism of fracturing imbibition, energy enhancement, and oil displacement to enhance oil recovery [16–18].

Imbibition is critical for the exploitation of hydrocarbon resources in tight oil reservoirs. Imbibition, driven by capillary forces, is where the wetting phase enters the pore, displacing the non-wetting phase. This process is crucial in determining the degree of oil production and recovery in tight oil reservoirs [19–21]. Spontaneous imbibition depends on the interaction between oil/water/rock multiphase flows. Imbibition usually involves complex forces between capillary, gravity, and viscous forces [10,22–24]. Spontaneous imbibition leads to low flow back rates in tight reservoirs as the fluid stays within the formation and is replaced by imbibition fluid due to capillary forces. Yu et al. conducted imbibition and oil displacement experiments on the same core, and verified the experimental results in combination with relevant models. Studies have shown that the macroscopic standard law is applicable to capillary imbibition [25–28]. Lyu et al. studied the effect of reservoir heterogeneity on spontaneous imbibition; the results show that the heterogeneity of permeability and wettability can change the water saturation distribution. More significant heterogeneity corresponds to a higher degree of spontaneous imbibition [29–31]. Tang et al. found that the factors affecting spontaneous imbibition were particle migration and initial water saturation [32]. Li et al. conducted a low salinity imbibition displacement experiment in an oilfield and confirmed the feasibility of low salinity fracturing fluid to enhance oil recovery [33]. Hou et al. studied the influence of confining pressure on spontaneous imbibition; the experimental results showed that confining pressure had an inhibitory effect on imbibition [34]. Qu et al. combined pore structure parameters with spontaneous imbibition mercury injection and imbibition experiments. The conclusion is that the higher the proportion of large apertures, the greater the amount of spontaneously imbibed liquid [35]. Tian et al. used traditional experimental methods to study the influence of different surfactant and standard saline solution formulations on the imbibition effect [36]. The experimental results show that combining cationic surfactant and normal saline can significantly improve the imbibition effect [37]. In addition, Schembre et al. investigated the relationship between seepage-absorption distance and saturation based on real-time characterisation of the distribution and morphology of the fluid by CT scanning and MRI. Using conventional experimental methods, Liu et al. tested the imbibition effects of alkaline water, NaCl solution, and nanofluids. The results show that the nanofluids perform well and can effectively enhance imbibition recovery [18]. Dou et al. studied the static imbibition experiment of tight reservoir core using nuclear magnetic resonance technology, analyzing the influence of permeability on the imbibition of a tight reservoir. The results indicate a positive correlation between matrix permeability and core imbibition recovery [13].

In addition, Xia et al. investigated changes in the wettability of carbonate reservoirs induced by cationic and anionic surfactants. They demonstrated that changing wettability through ion formation is more effective than absorbing anions from surfactants [23]. Qin et al. studied the effect of non-ionic surfactants on the wettability of the calcite surface. The conclusion is that wettability is altered through surfactant coating and oil cleaning [38]. Based on nuclear resonance technology, Li et al. conducted relevant experiments on the structure characteristics of tight pores and the distribution of pore crude oil at different imbibition stages. The results indicated that micropores facilitated the imbibition recovery of most crude oil, while nano-pores exhibited the highest imbibition efficiency due to the substantial capillary force [39]. Cao et al. found that the smaller the ratio of oil viscosity to water viscosity, the better the dynamic imbibition effect. The higher the initial water saturation, the worse the dynamic imbibition effect [40–43]. Based on the CT online experimental system, Yang et al. explored the influence of pressure, permeability, and initial water saturation on imbibition distance according to changes in core water saturation during imbibition [44]. Ren et al. investigated the imbibition recovery of carbonated water under high-pressure conditions through experimental design [45]. The research results showed that due to the unique properties of carbonated water, carbon dioxide diffusion also existed in the imbibition process to improve the imbibition recovery [45–47].

Previous studies have predominantly concentrated on the imbibition of water and surfactants under normal temperature and pressure conditions. However, there is limited research on the imbibition behavior of fracturing fluids at high temperatures and pressures. In this paper, imbibition experiments in tight reservoirs were conducted using a nuclear magnetic resonance experimental device, exploring the imbibition effects of fracturing fluid under various temperatures, pressures, and matrix permeability conditions. Furthermore, based on the division of pore structure in the experimental core, each pore's recovery in the imbibition process was quantitatively analyzed, and the mobilization law of each pore under different experimental conditions was revealed.

2. Experiments

This section describes the reservoir characteristics of the study block, formation water, crude oil properties, experimental cores, types of imbibition fluids, and experimental setup.

2.1. Reservoir Rock

Target reservoir: In this paper, the Ordos Chang 8 reservoir is taken as the study block, with a burial depth ranging from 1600 m to 4000 m, an average permeability of 0.01 mD to 2 mD, an oil saturation of 55% to 63%, a porosity ranging from 5% to 12%, and a formation pressure of 15 MPa.

Experimental core: To investigate the imbibition effect of fracturing fluids in tight reservoirs, 11 cores of Ordos Chang 8 reservoir were selected for imbibition experiments in this paper. The permeability and porosity of the experimental cores were determined using the PDP-200 instrument, the experimental setup was purchased from Jiangsu Tuochuang Company in Nanjing, China. With the core permeability ranging from 0.04 mD to 0.3 mD and porosity ranging from 9% to 12%, typical of tight sandstone reservoirs. Specific parameters of the experimental core are shown in Table 1.

Table 1. The properties of experimental cores.

No.	Porosity (%)	Permeability (mD)	Diameter (cm)	Length (cm)
A1	11.21	0.230	2.528	4.992
A2	11.08	0.225	2.526	5.012
A3	10.49	0.216	2.526	5.024
A4	10.89	0.232	2.526	4.991
A5	9.64	0.111	5.530	5.022
A6	9.45	0.120	2.530	4.991
A7	9.89	0.115	2.530	5.051
A8	5.05	0.04	2.526	4.992
A9	7.32	0.08	2.526	5.044
A10	9.89	0.114	2.530	4.992
A11	10.35	0.253	2.530	5.011

2.2. Fluids

Fracturing fluid: The CNI-A fracturing fluid used in the experiment was provided by Changqing oilfield. The volumetric concentration of the fracturing fluid is 0.8 L/m³, and the interfacial tension is 0.89 mN/m.

The rotating droplet method determined the interfacial tension between CNI-A surfactant and crude oil using a dynamic interfacial tensiometer. The dynamic interfacial tensiometer consists of a rotating system, a setting system, a temperature control system, and an analysis software. When the rotating droplet method is used to determine the interfacial tension, the centrifugal tube of the rotating interfacial tensiometer contains two kinds of liquids, low-density phase (crude oil) and high-density, and the crude oil exists in the form of droplets in the surfactant solution. When rotating at a high speed, the liquid of the low-density phase is stretched and deformed due to centrifugal force. When the interfacial tension, gravity, and centrifugal force reach equilibrium, the interfacial tension

can be calculated by Equation (1). The contact angle was measured on an experimental core of 0.115 mD, at a temperature of 20° and a pressure of 0 MPa. Through experimental studies, the temperature and pressure have not yet had an effect on the contact angle.

$$\sigma = \frac{\Delta\rho\omega^2R^3}{4} \quad (1)$$

σ Interfacial tension mN/m.

ω Angular velocity rad/s.

R radius μm .

$\Delta\rho$ oil-water density difference kg/m^3 .

The contact angles were measured using the JY-PHb Contact Angle Tester, the experimental setup is due to be manufactured by Chengde Jinhe Instrument Manufacturing Company in Shijiazhuang, Hebei Province, China. The contact angle is a method of dropping a drop of liquid, satisfying the required volume on a solid surface, and measuring or calculating the contact angle of the solid surface through image analysis. The JY-PHb contact angle tester consists of an injection system, a filming system, a sample platform, and analysis software. Wetting angle measurements were carried out using crude oil from the stratum and core of the target block. The experimental results are shown in Figure 1. As can be seen from the figure, the contact angle becomes smaller after percolation, indicating that the CNI fracturing fluid can change the core wettability and improve the percolation effect.

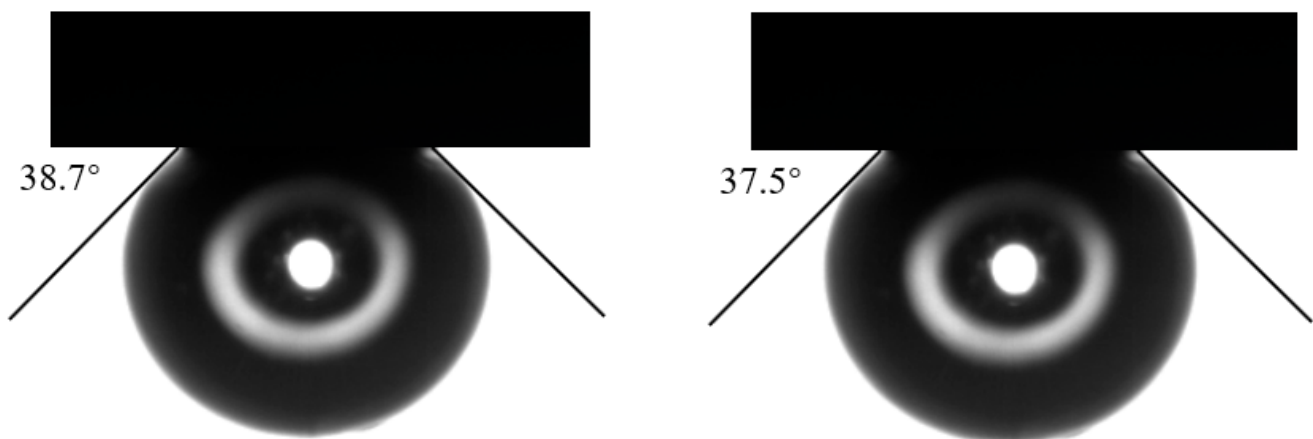


Figure 1. Wettability test results.

Crude oil: The crude oil used in this study was sourced from the same field. At a temperature of 25 °C and atmospheric pressure, the oil has a viscosity of 1.76 mPa s and a density of 0.714 g/cm³. The compositional content of surface-degassed crude oil is shown in Figure 2.

Formation water: The total salinity of the formation water is 30,000.9 mg/L, and the components and properties of the formation are shown in Table 2. The formation water was prepared in the experiment based on its ionic composition and salinity.

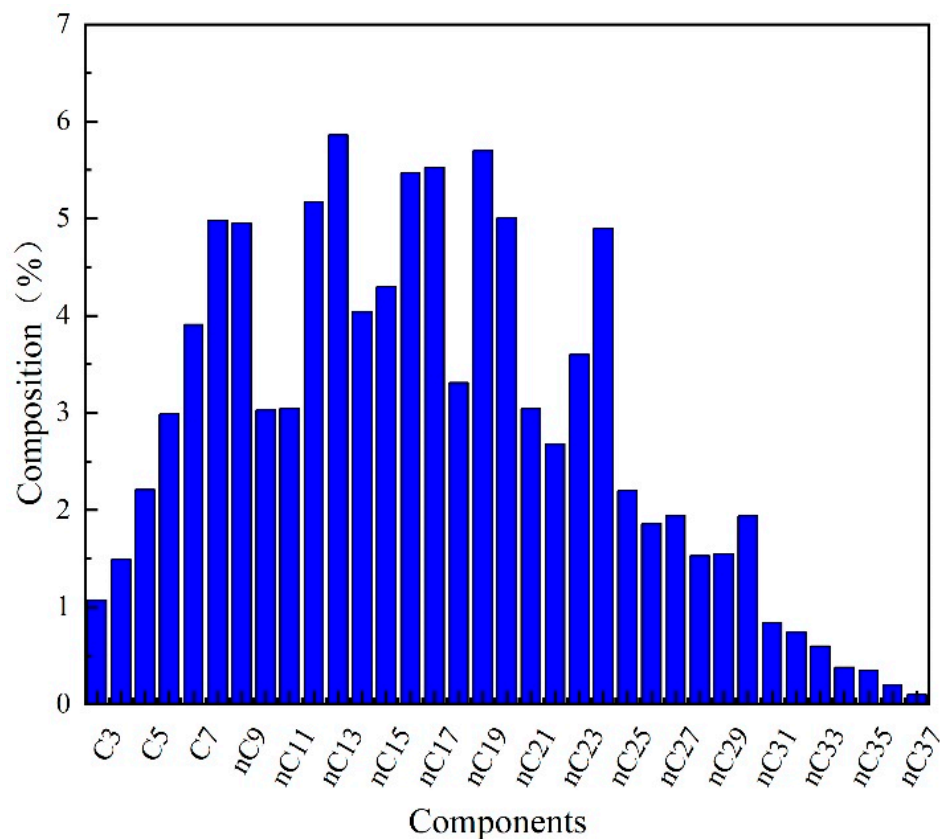


Figure 2. Component content of surface-degassed crude oil.

Table 2. The components and properties of artificial formation water.

Total Salinity, mg/L	K ⁺ , Na ⁺	Ca ²⁺	Mg ²⁺	Cl ⁻	SO ₄ ²⁻	HCO ₃ ³⁻
30,000.9	20,390	2601	352	36,028	1100	370

2.3. Experimental Setup and Process

2.3.1. Experimental Setup

This section describes the critical instrumentation in the CNI-A fracturing fluid imbibition experiment. The device selected for the core imbibition experiment is an imported high-temperature and high-pressure repelling system, with the pressure range of the repelling pump from 0 to 50 MPa, the continuous flow rate of the pump from 0.001 to 100 mL/min, and the accuracy of the pressure and speed up to 0.3%. Wuhan Petroleum Company Limited (Wuhan, China) provides the intermediate vessel and has a pressure resistance of 50 MPa. The core imbibition analysis device is an imported nuclear magnetic resonance (NMR) analyzer with a model number of MesoMR23-060H-1, the experimental device was manufactured by Shanghai Newmax Electronic Technology Company in Shanghai, China. a resonance frequency of 21.242 MHz, a probe coil of 25 mm, an echo time of 0.27 ms, and a scanning frequency of 64 times. The experimental setup is shown in Figure 3.

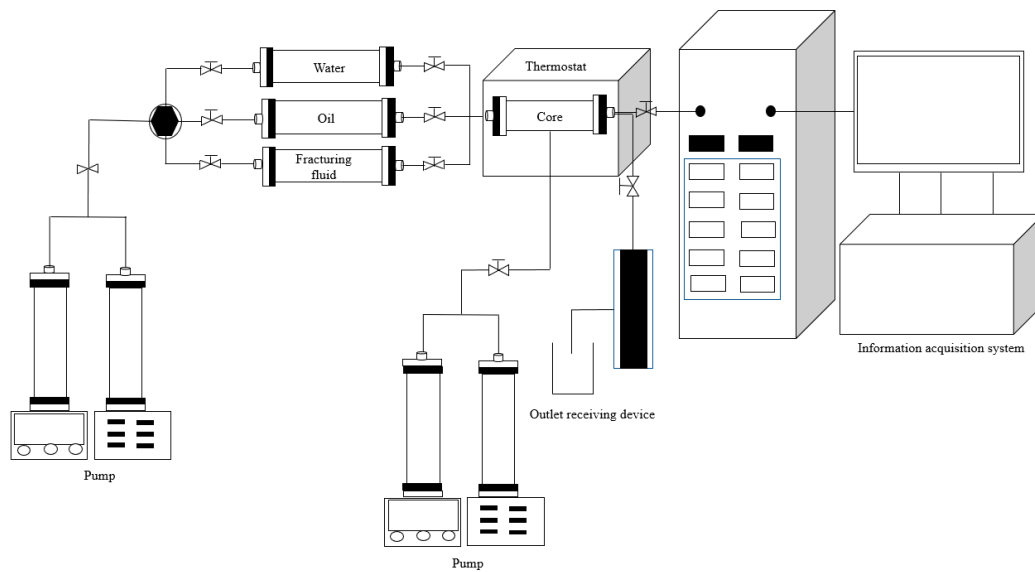


Figure 3. Experimental setup.

2.3.2. NMR

Experimental studies on imbibition in tight reservoir cores typically employ mass and volume methods to calculate the recovery degree. Although these methods allow for comparing imbibition effects under different parameters, they do not provide a quantitative analysis of the mobilization law for each pore space during the imbibition process. NMR experiments offer advantages such as visualization, fast monitoring, non-destructive monitoring, and accurate metrology, allowing for detecting the core imbibition process through T_2 spectrum analysis [29].

The principle of nuclear magnetic resonance involves utilizing the resonance phenomenon between the electrons in the atoms of the substance under test and the applied magnetic field. This allows for testing the sample and obtaining the content of the substance under examination by measuring the intensity of the obtained signal. The process of the atomic nucleus recovering from the high energy state of resonance excited by the applied magnetic field to the low energy state is called the relaxation time, which is another significant physical quantity for NMR testing, encompassing both longitudinal relaxation and transverse relaxation. As the hydrogen atoms in the oil and water within the core possess a nuclear magnetic moment, they undergo continuous rotation, leading to resonance under the influence of the applied magnetic field. The signal strength is more vital for materials with a greater mass of hydrogen. In order to facilitate the analysis of the experiment, deuterium water is used in this paper's experimental process to eliminate the impact of the water signal and study the simulation of signal changes in the oil. Due to the complexity of the oil–water distribution characteristics within the rock pore space and the influence of the pore structure, the oil–water interface is divided by rock boundaries with different shapes and boundary properties. This division results in unequal chances of contact between hydrogen nuclei within the fluid and the solid surface. Therefore, the relaxation time profile can reflect the fluid distribution in different rock pore sizes [30].

This section proposes the calculation method for quantitatively evaluating the effect of fracturing fluid imbibition. As mentioned in the previous subsection, since the relation between the T_2 value of nuclear magnetic resonance and pore radius is a power function, the pore distribution can be categorized into three grades: micropores (0.01 ms~10 ms), mesopores (10 ms~100 ms), and macropores (>100 ms). Simultaneously, the imbibition effect of fracturing fluid in different pores was quantitatively evaluated according to Formula (2). Firstly, the core NMR T_2 curve of the initial saturated oil state of the sample is obtained, and then the NMR scanning is carried out at the set imbibition time to obtain the T_2 spectra at different times, and then the imbibition recovery is calculated by using

Formula (2) with the change of the area of the T_2 spectra at different times. In addition, according to the delineated pore structure, the area change during the imbibition process of each pore was calculated, and the different pore recoveries were calculated.

$$R = \frac{S_0 - S_1}{S_0} \times 100\% \quad (2)$$

where R is the oil recovery efficiency of fracturing fluid imbibition under capillary force, %. S_0 is an area of the T_2 spectrum peak with no imbibition, and S_1 is the area of the T_2 spectrum peak after imbibition.

2.3.3. Experimental Procedure

In order to explore the influence of temperature, pressure, and matrix permeability on the imbibition effect, 11 tight cores were selected to conduct experiments. The specific experimental scheme design is shown in Table 3.

- (1) The cores were cleaned and dried until a constant mass was achieved. Subsequently, the essential parameters of each core were measured, encompassing core length, diameter, permeability, and dry weight.
- (2) The experimental cores underwent a vacuum saturated with water using the evacuation method. Subsequently, the original pore distribution of the experimental cores was acquired using an NMR scanner.
- (3) After measuring the T_2 spectrum, the core was saturated with water, evacuated, and saturated with deuterium water to shield the water signal in the core.
- (4) Bound water was established by driving simulated crude oil, and the core was saturated with oil when the total liquid volume at the outlet was 10 PV, and saturated oil T_2 spectra were obtained by the NMR scanning unit. The cores were then aged for 15 days.
- (5) To mitigate the interference of the hydrogen signal from the fracturing fluid, deuterium water was used to configure the fracturing fluid in this experiment, ensuring that only the oil signal changed during the experiment.
- (6) The initial imbibition occurs rapidly with short measurement intervals, while the later imbibition slows down and the measurement interval increases. These steps are repeated until the NMR T_2 spectrum no longer changes.
- (7) Quantitative analysis of recovery under different conditions using different time NMR T_2 curves to reveal different pore mobilization patterns.

Table 3. Experimental schemes.

No.	Porosity (%)	Permeability (mD)	Experimental
A1	11.21	0.230	Pressure
A2	11.08	0.225	
A3	10.49	0.216	
A4	10.89	0.232	
A5	9.64	0.111	Temperature
A6	9.45	0.120	
A7	9.89	0.115	
A8	5.05	0.04	Permeability
A9	7.32	0.08	
A10	9.89	0.114	
A11	10.35	0.253	

2.3.4. Technical Lines of Research

In this paper, we firstly analyze the reservoir characteristics of the research block, and select reasonable experimental cores according to the structural characteristics of the reservoir, and complete the pre-processing before the experiment. Secondly, we design the

experimental programme and adjust the experimental device according to the research content. Finally, the influence of different factors on imbibition and absorption is analyzed with the experimental data. The technical route of the study is shown in Figure 4.

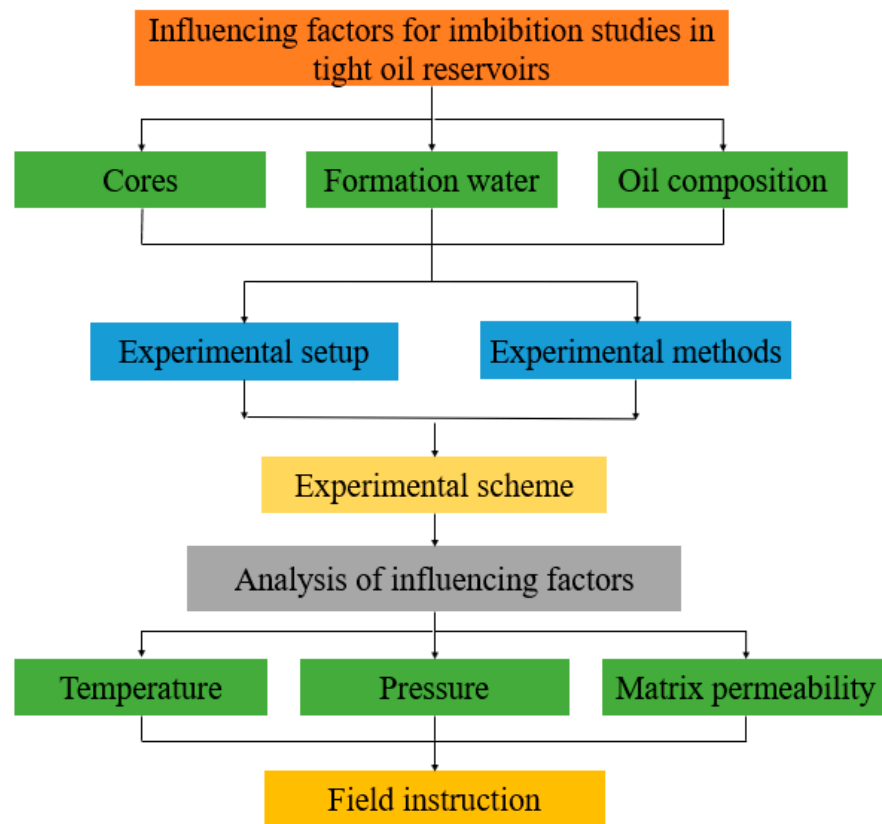


Figure 4. Technical lines of research.

3. Results and Discussion

This part explores the effects of matrix permeability, temperature, and pressure on the effect of imbibition based on experimental results. The pores were classified into micropores, mesopores, and macropores according to the relaxation time, and the recovery of each pore in the process of imbibition was quantitatively analyzed.

3.1. Distribution Characteristics of T_2 Spectra of Different Cores

This part describes the T_2 spectra of experimental cores in the initial saturated oil state. By comparing the differences in T_2 spectra in 11 experimental cores, the pore size and fluid distribution characteristics of the tight reservoirs are determined. Figure 5 indicates the T_2 spectra of the experimental cores, in which A1, A2, A3, A4, A7, A8, A9, and A10 are single peak distribution and A5, A6, A11 are double peak distributions. The distributions of the experimental cores are all in the range of 0.01 ms to 1200 ms, with single peaks in the range of 10 ms to 100 ms, and double peaks in the range of 0.1 ms to 1 ms and 10 ms to 100 ms; micropores and mesopores mainly dominate the cores. The double peaks are distributed as high left fronts and low right peaks, which are more non-homogeneous and structurally complex compared to the single peaks.

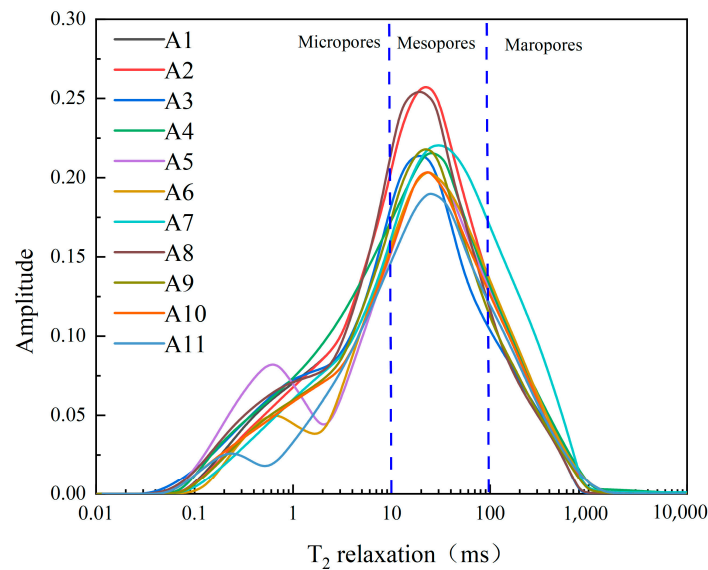


Figure 5. Saturated oil T_2 spectra of core samples.

3.2. Pressure

In this study, we performed CNI-A fracturing fluid imbibition experiments on four groups of core samples at different pressures to investigate the effect of pressure on imbibition. The four experimental pressures were 15 MPa, 10 MPa, 5 MPa, and 0 MPa, respectively. The experimental temperature was 40 °C. The NMR curves at different experimental pressures are shown in Figures 6–9. The highest imbibition recovery of CNI-A fracturing fluid was 27.0% at the experimental pressures of 15 MPa, 10 MPa, and 5 MPa, and the lowest imbibition recovery was achieved at the pressure of 0 MPa. The NMR curves under different experimental pressures show a consistent pattern; with the increase of the imbibition time, the signal amplitude of the NMR curves gradually decreases, and the range of relaxation time gradually narrows. The NMR curve decreased the fastest in the early stage, decreased gradually in the middle stage, and the curve remained constant in the late stage.

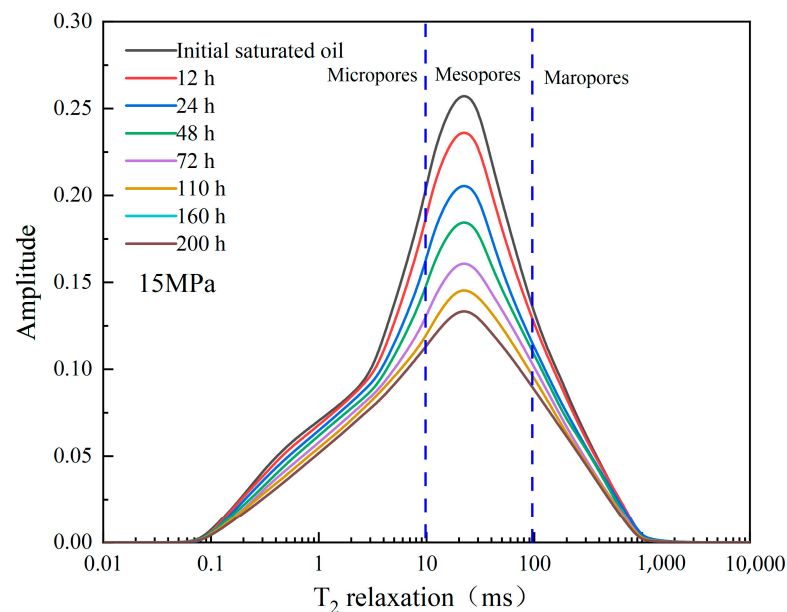


Figure 6. Experimental pressure of 15 MPa imbibition NMR curves.

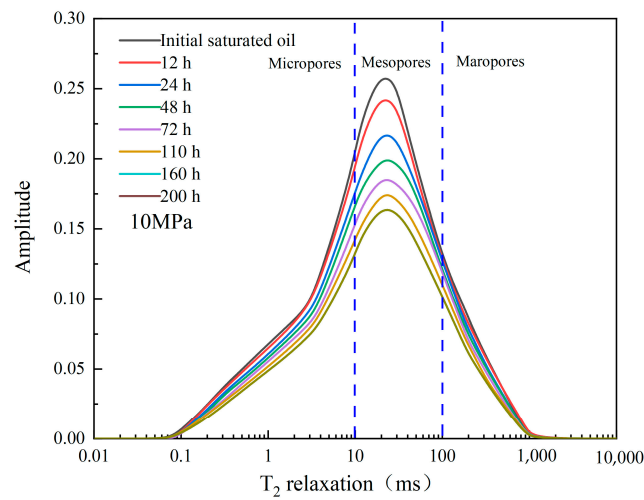


Figure 7. Experimental pressure of 10 MPa imbibition NMR curves.

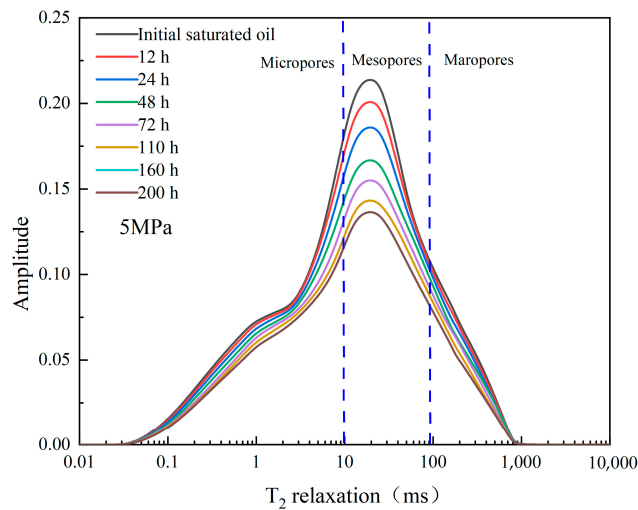


Figure 8. Experimental pressure of 5 MPa imbibition NMR curves.

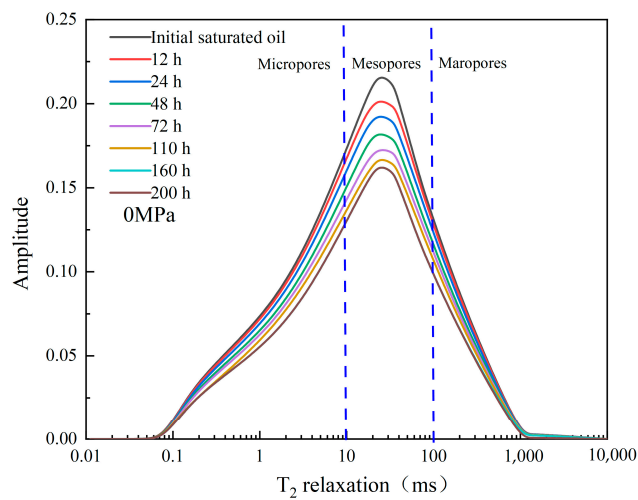


Figure 9. Experimental pressure of 0 MPa imbibition NMR curves.

According to Figures 10 and 11, the imbibition recovery curve can be divided into three stages: fast, slow, and imbibition equilibrium. In the early stage, the strong capillary force facilitates the entry of fracturing fluid into the core, increasing the chances of contact

with crude oil and leading to the fastest recovery rate. During the middle stage, as water saturation rises, the influence of capillary force diminishes, resulting in a slower increase in the recovery rate. In the later stage, the reduced capillary force is insufficient to drive crude oil within the core, leading to the attainment of imbibition equilibrium. In addition, from the change in the imbibition recovery curve, in the range of experimental pressure from 0 to 5 MPa, the imbibition recovery gradually becomes more significant with the increase of experimental pressure. In the experimental pressure range of 5 to 15 MPa, the imbibition recovery remained constant with the increase in pressure.

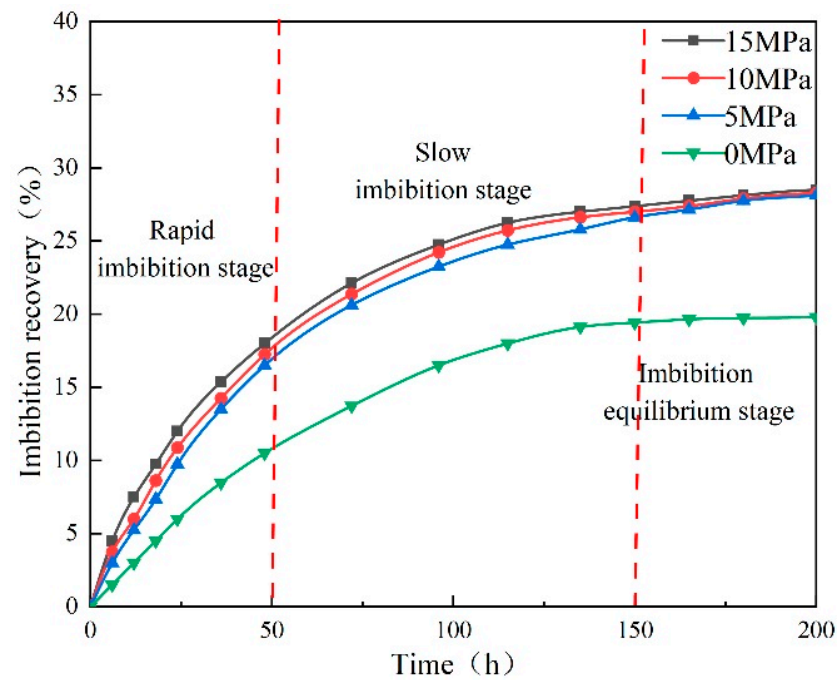


Figure 10. Imbibition recovery curves at different experimental pressures.

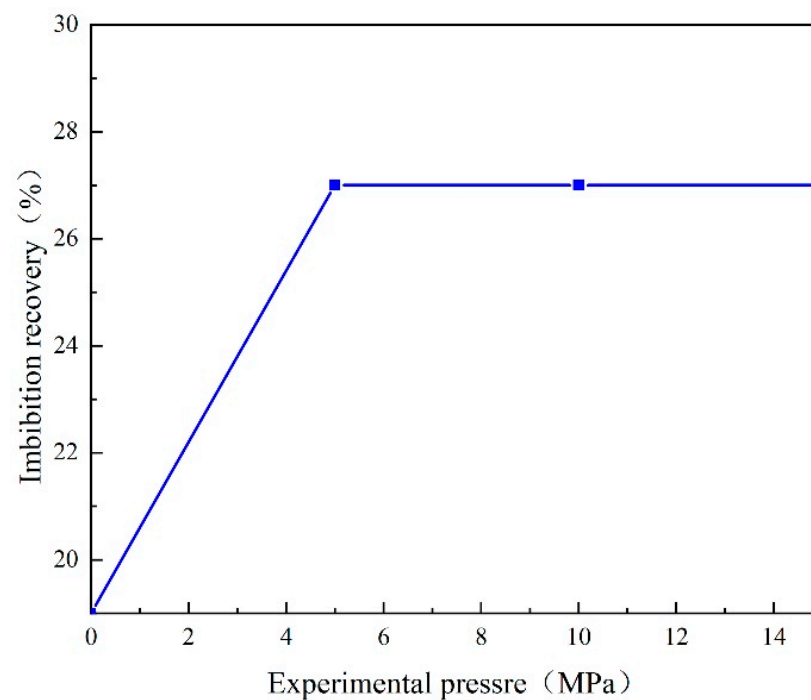


Figure 11. Pressure versus imbibition recovery curves.

To analyze pressure's impact on fracturing fluid percolation recovery further, we compared the degree of mobilization of each pore at different experimental pressures (Figures 12–15). The experimental results reveal a consistent pattern in the mobilization degree of each pore space under varying pressures, with micropores exhibiting the highest degree of mesopores and macropores displaying the lowest. The utilization pattern of each pore space aligns with the observed change in imbibition recovery at the experimental pressures of 5, 10, and 15 MPa. Compared to the pressures of 5, 10, and 15 MPa, the utilization degree of each pore space decreases at 0 MPa.

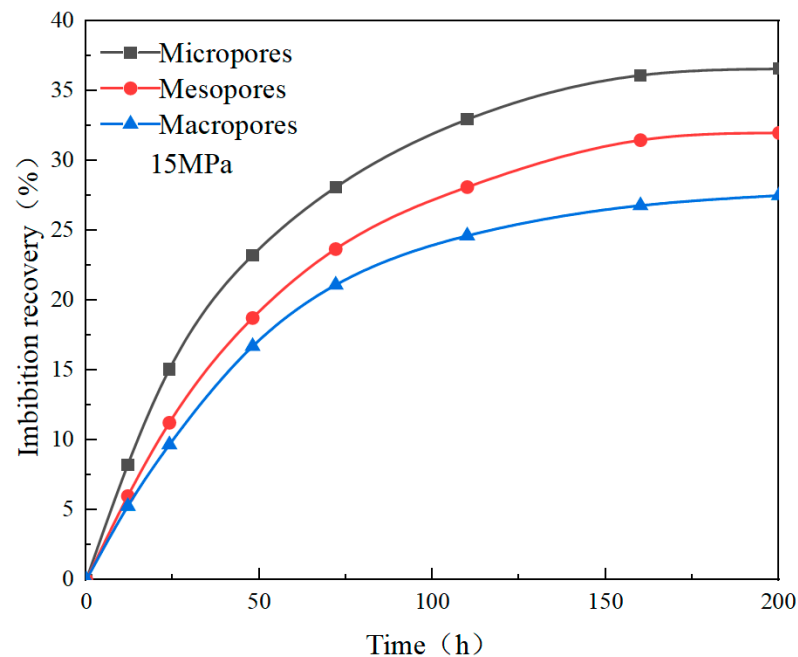


Figure 12. Experimental pressure of 15 MPa different pore imbibition recovery.

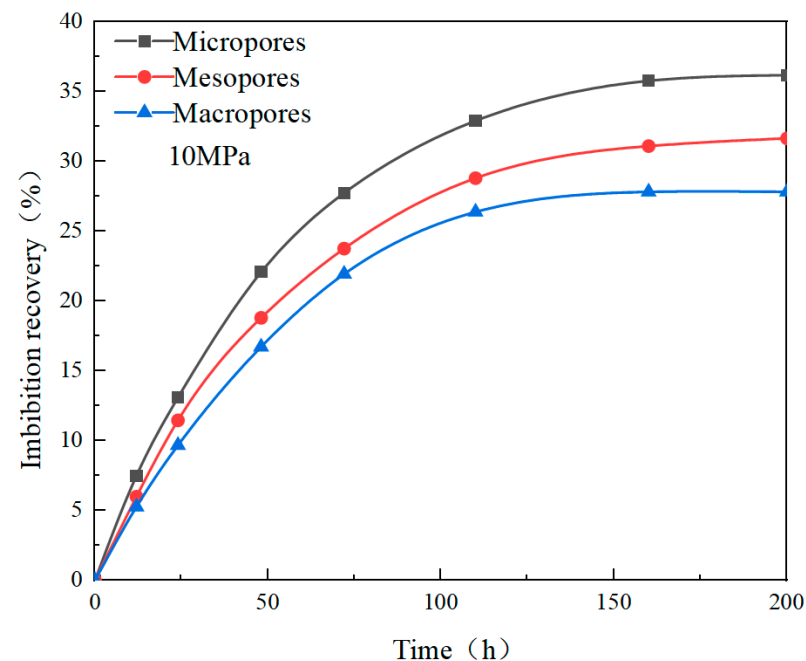


Figure 13. Experimental pressure of 10 MPa different pore imbibition recovery.

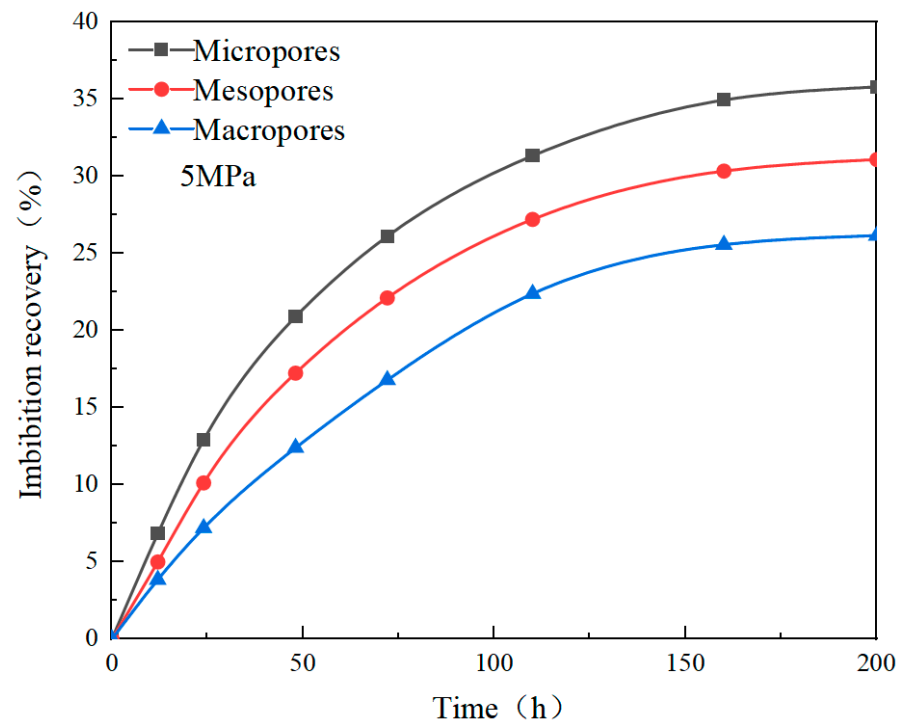


Figure 14. Experimental pressure of 5 MPa different pore imbibition recovery.

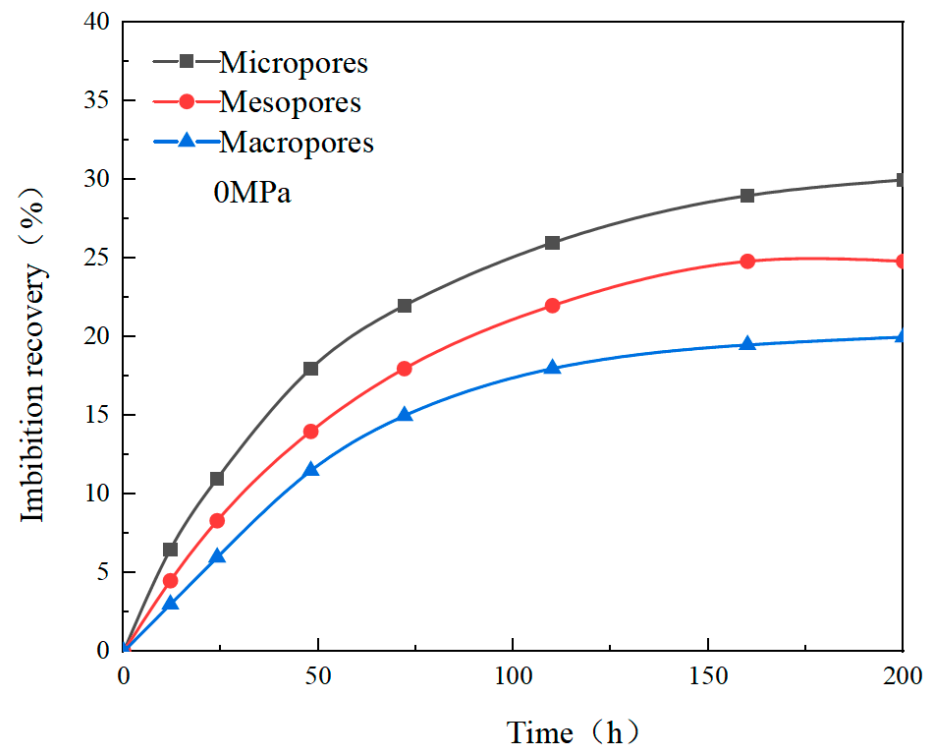


Figure 15. Experimental pressure of 0 MPa different pore imbibition recovery.

There are two primary reasons. Firstly, the capillary force is the principal driving factor in the imbibition process, with the pore radius being a key determinant. Reasonable experimental pressure (5 MPa) will promote the flow of fracturing fluid to the internal pores of the core, so as to seep and replace more crude oil in the core pores; at the same time, due to the action of pressure, the volume compression of the core pores will cause the crude oil in the pores to be squeezed and discharged, which will improve the recovery of imbibition

to a certain extent. Secondly, when the experimental pressure exceeds 5 MPa, the pore radius diminishes due to external compression of the pores. Although this compression elevates the capillary force, the fluid flow resistance surpasses the capillary force, inhibiting imbibition. At high experimental pressures, the initial recovery rate increases rapidly, but the subsequent recovery diminishes more noticeably. Hence, within a reasonable range, elevating the experimental pressure facilitates the ingress of the wetting phase into smaller core matrices, thereby enhancing imbibition recovery. Additionally, during the imbibition process, the highest recovery occurs in micropores, while macropores exhibit the lowest recovery due to the combined effects of capillary force and experimental pressure. Within a reasonable range, as the experimental pressure increases, the recovery of each pore also increases. However, beyond this range, pore resistance induced by high experimental pressure surpasses the flow-driving force, halting further improvement in pore recovery. Consequently, in practical production, selecting an optimal pressure range to leverage the seepage and suction effects is essential, thereby maximizing the recovery of tight reservoirs.

3.3. Temperature

This section was conducted to investigate the effect of temperature on the imbibition of CNI-A fracturing fluids. The experimental temperatures were 20 °C, 40 °C, and 60 °C, and the experimental pressure was 5 MPa. The NMR curves at different experimental temperatures are shown in Figures 16–18, and the area of the NMR curves gradually decreases with the increase of time. The curve variations observed at different experimental temperatures follow a consistent pattern, characterized by the most significant decrease in curve area during the early stage, a gradual decrease in the middle stage, and a stable area in the late stage. The core imbibition recovery results at different temperatures are illustrated in Figure 19. It can be seen from the figure that the final imbibition recovery of the S5 core at room temperature is 19.56%. When the temperature increases to 40 °C, the core imbibition recovery efficiency increases to 23.74%, which is 4.18% higher than the normal temperature. When the experimental temperature is increased to 60 °C, the core imbibition recovery efficiency is increased to 27.58%, which is 3.84% higher than that of 40 °C. According to the analysis of the imbibition curve, when the experimental temperature is 60 °C, the imbibition recovery is the highest, and the imbibition equilibrium time is the shortest. When the experimental temperature is 20 °C, the imbibition recovery is the lowest, and the imbibition equilibrium time is the longest.

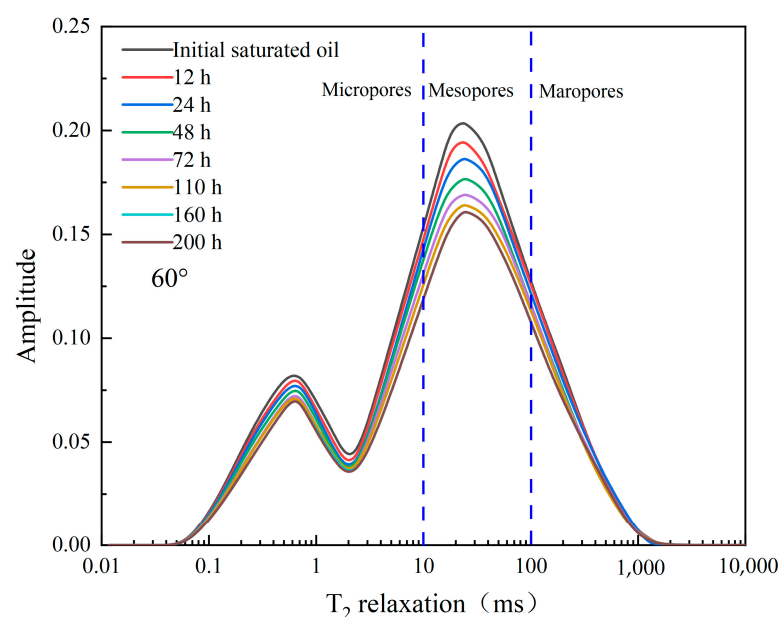


Figure 16. Experimental temperature of 60 °C imbibition curves.

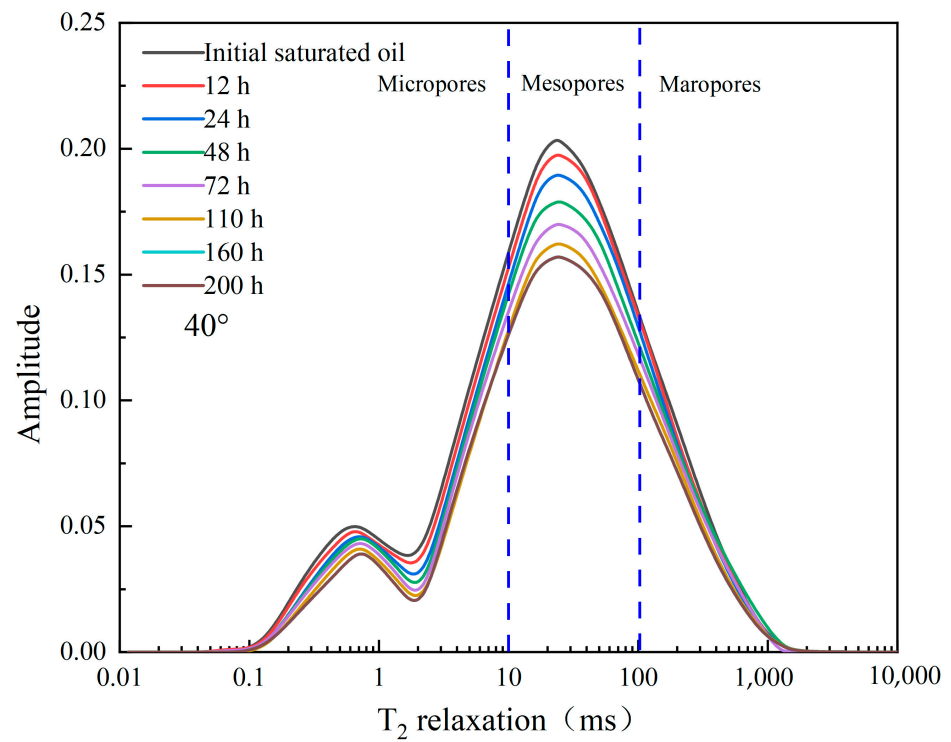


Figure 17. Experimental temperature of 40 °C imbibition curves.

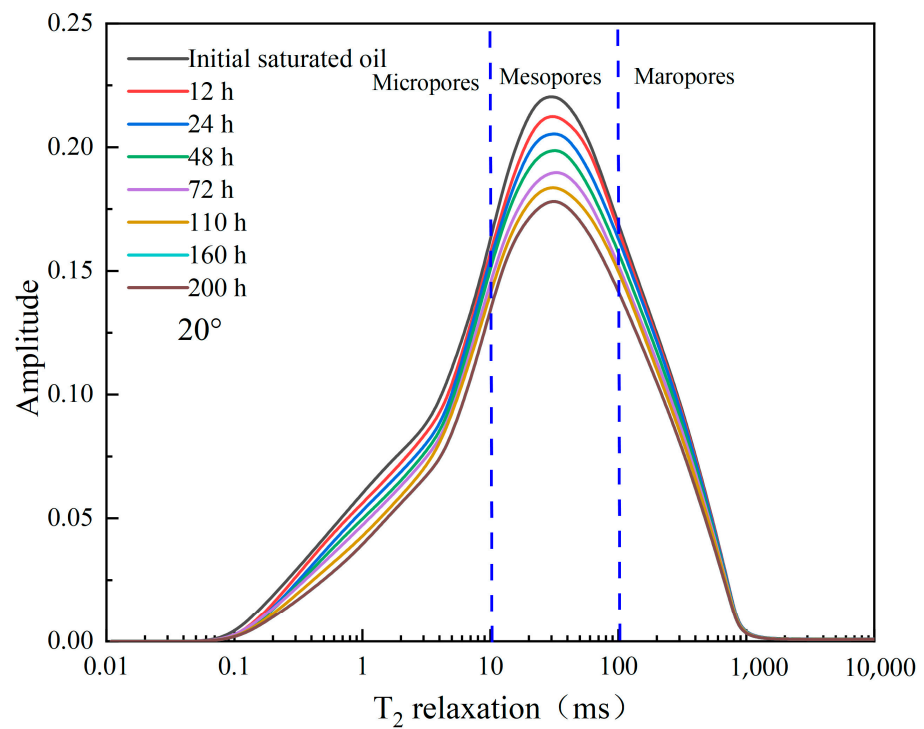


Figure 18. Experimental temperature of 20 °C imbibition curves.

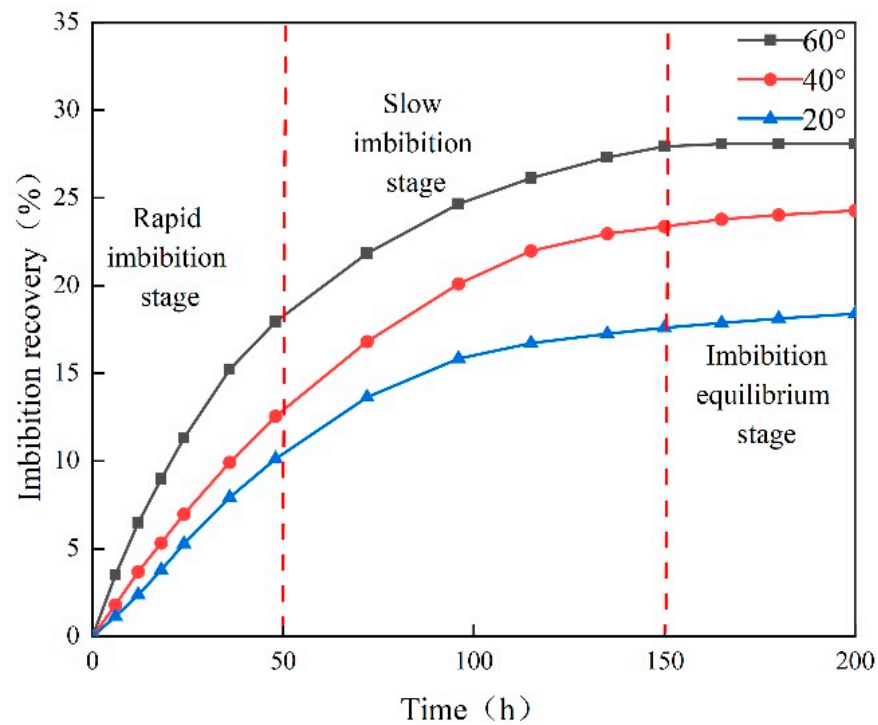


Figure 19. Imbibition recovery curves at different experimental temperatures.

In addition, the process is divided into a fast imbibition stage, a slow imbibition stage, and an imbibition equilibrium stage based on the change in the fracturing fluid imbibition recovery curve. The higher the temperature, the faster the rate of increase of recovery in the fast imbibition stage and slow imbibition stage, and the shorter the time to reach imbibition equilibrium. Conversely, the lower the temperature, the smaller the rate of increase in recovery and the longer the time to reach imbibition equilibrium.

To further investigate the effect of experimental temperature on the imbibition of fracturing fluid, the recovery of each pore under different experimental temperatures was comparatively analyzed. The experimental results are shown in Figures 20–22. Upon analyzing the results, it is evident that micropores exhibit the highest recovery, followed by mesopores, with macropores displaying the lowest recovery under various experimental temperatures. Additionally, as the experimental temperature decreases, the recovery of each pore gradually diminishes, aligning with the observed pattern in the NMR curve changes. The main reason is that the influence in temperature on imbibition is manifold. On the one hand, the increase of temperature reduces the viscosity of crude oil, and the fluid fluidity is improved, which is conducive to the imbibition of oil and water. Meanwhile, crude oil tends to expand under high-temperature conditions, which increases the volume difference between crude oil and formation rocks, making it easier for crude oil to peel off the rock surface. On the other hand, as the temperature rises, the interior of the core is heated, increasing the elastic energy and allowing the fluid to drain outwards, promoting imbibition.

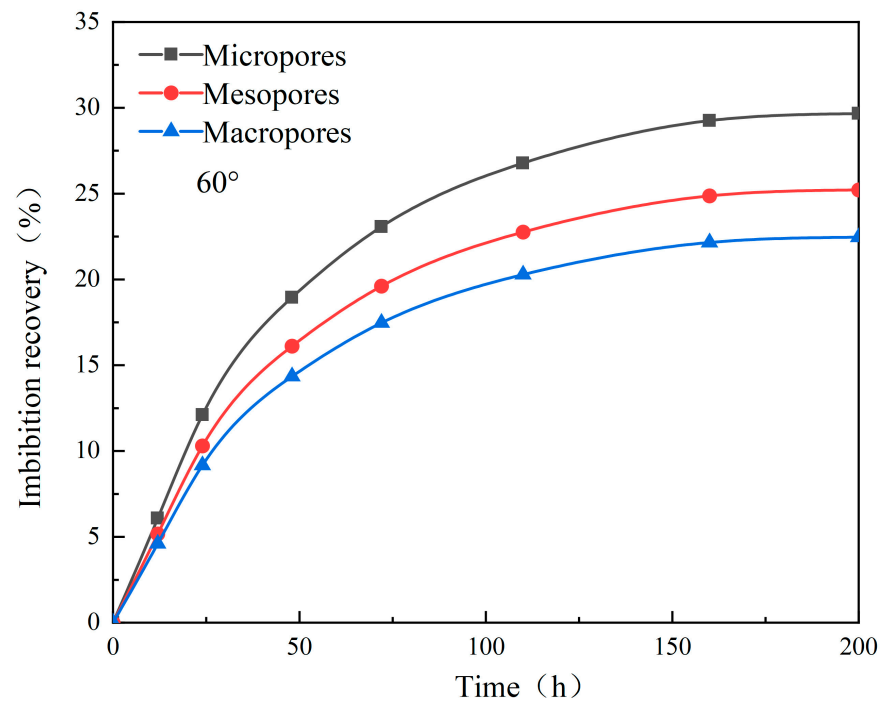


Figure 20. Different pore imbibition recovery curves.

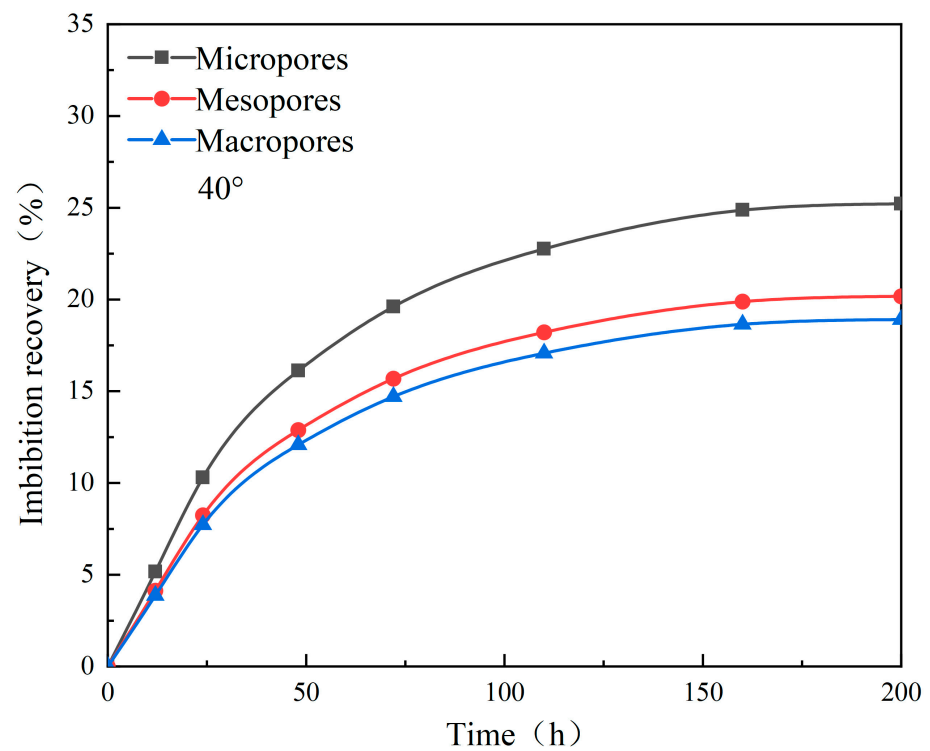


Figure 21. Different pore imbibition recovery curves.

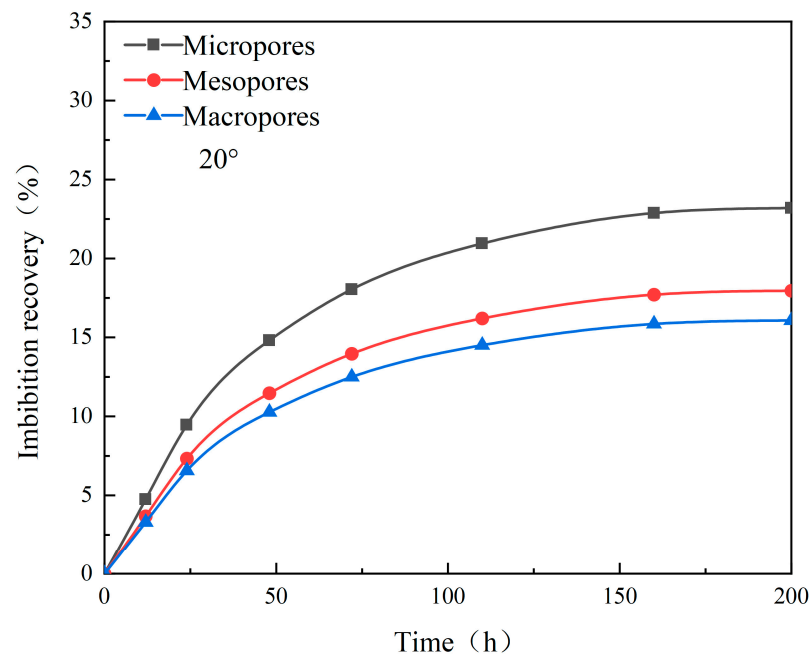


Figure 22. Different pore imbibition recovery curves.

3.4. Matrix Permeability

In order to study the effect of matrix permeability on the imbibition of fracturing fluids, four sets of matrix permeability imbibition experiments were carried out in this paper, with experimental pressures and temperatures of 5 MPa and 60°, respectively. NMR curves for cores with different matrix permeabilities are shown in Figures 23–26. As can be seen from the figure, the immersion NMR curves at different matrix permeabilities show a consistent variation. The signal intensity of the curves experiences the most rapid decrease in the early stage, attributed to the prevailing capillary force. This reduction slows down in the middle stage, ultimately stabilizing in the late stage. Within the scope of this experimental study, the more significant the matrix permeability, the greater the decrease in curve amplitude, which is consistent with the change in imbibition recovery. The experimental results are shown in Figure 27. The permeability of core S8 is 0.04 mD, and the final imbibition recovery is 16.51%. The permeability of core A 9 is 0.08 mD, and the final imbibition recovery is 20.32%; compared with A8, the imbibition recovery increased by 3.81%. The permeability of core A 10 is 0.11 mD, and the final imbibition recovery is 26.46%, which is 6.14% higher than that of A 9. The permeability of core S11 is 0.25 mD, and the final imbibition recovery is 29.75%, which is 3.29% higher than that of A 10. Analyzing the change in the recovery curve reveals that the imbibition of fracturing fluid with different matrix permeability can be categorized into three stages: fast imbibition, slow imbibition, and imbibition equilibrium. The rapid imbibition stage corresponds to the early phase, characterized by the most substantial influence of capillary force. Slow imbibition represents the middle stage, marked by increased water saturation and heightened seepage resistance, reducing the impact of the capillary. The imbibition equilibrium is in the late stage; the capillary force is insufficient to replace the matrix crude oil by imbibition, and the recovery remains constant.

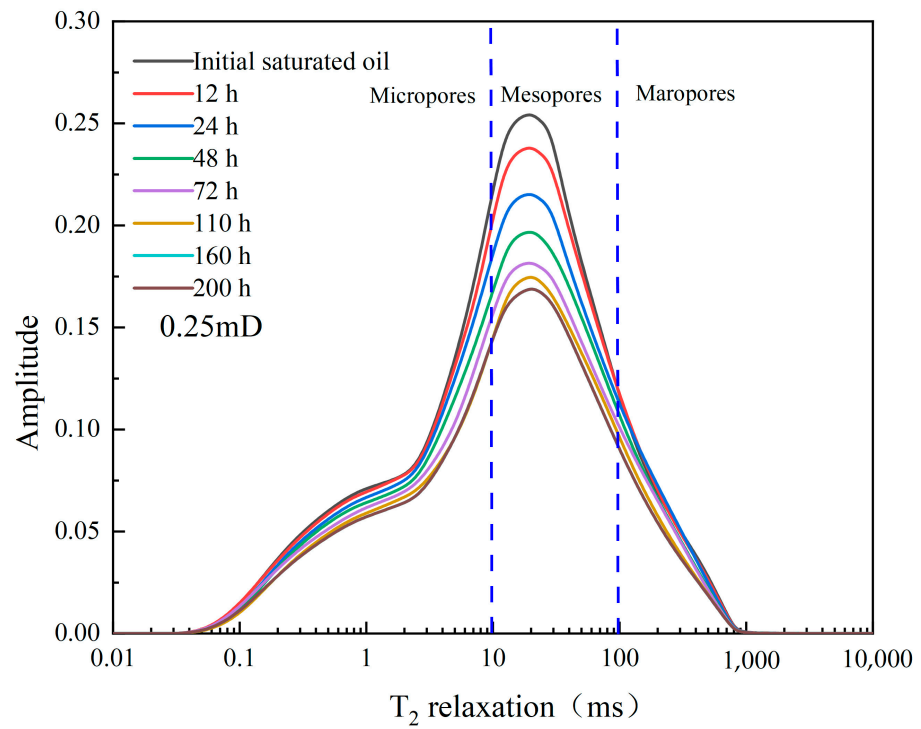


Figure 23. Matrix permeability of 0.25 mD imbibition NMR curves.

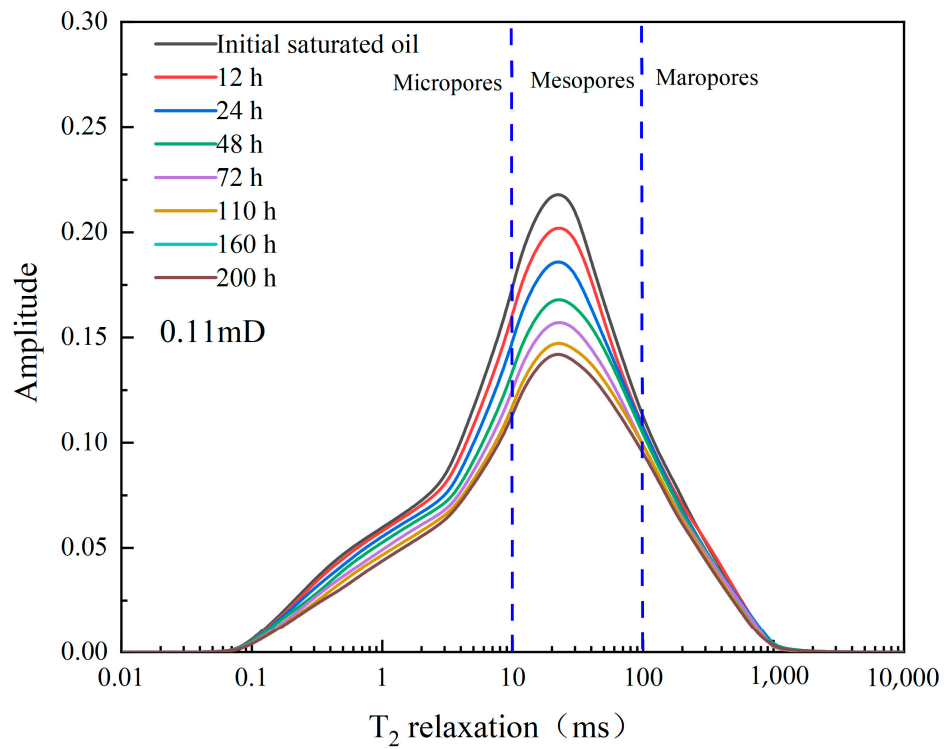


Figure 24. Matrix permeability of 0.11 mD imbibition NMR curves.

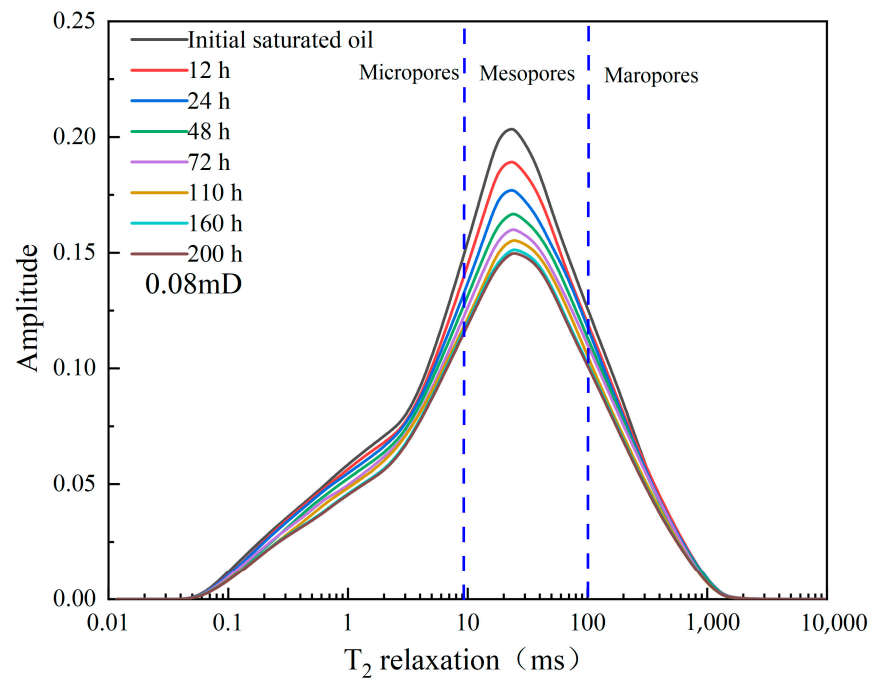


Figure 25. Matrix permeability of 0.08 mD imbibition NMR curves.

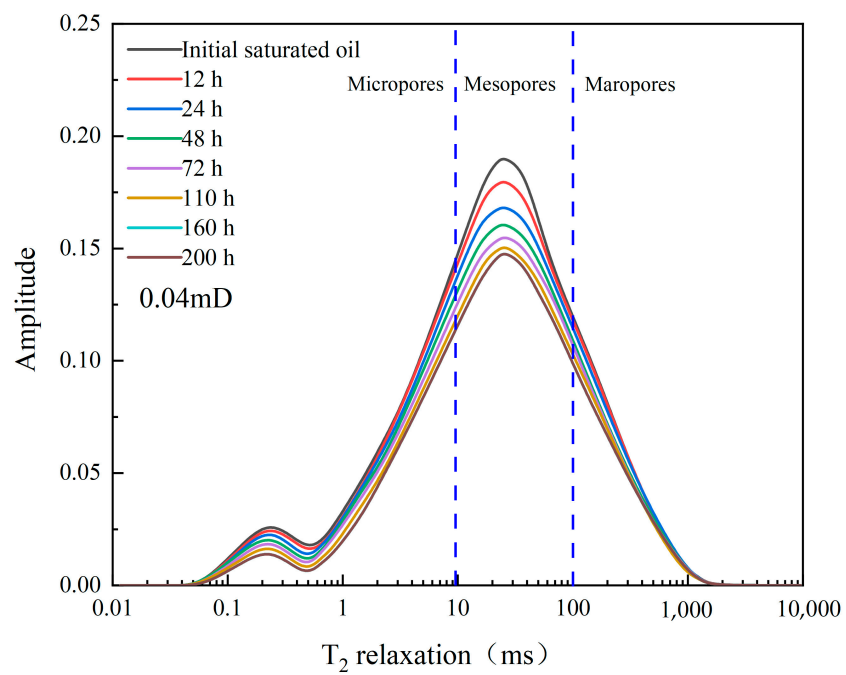


Figure 26. Matrix permeability of 0.04 mD imbibition NMR curves.

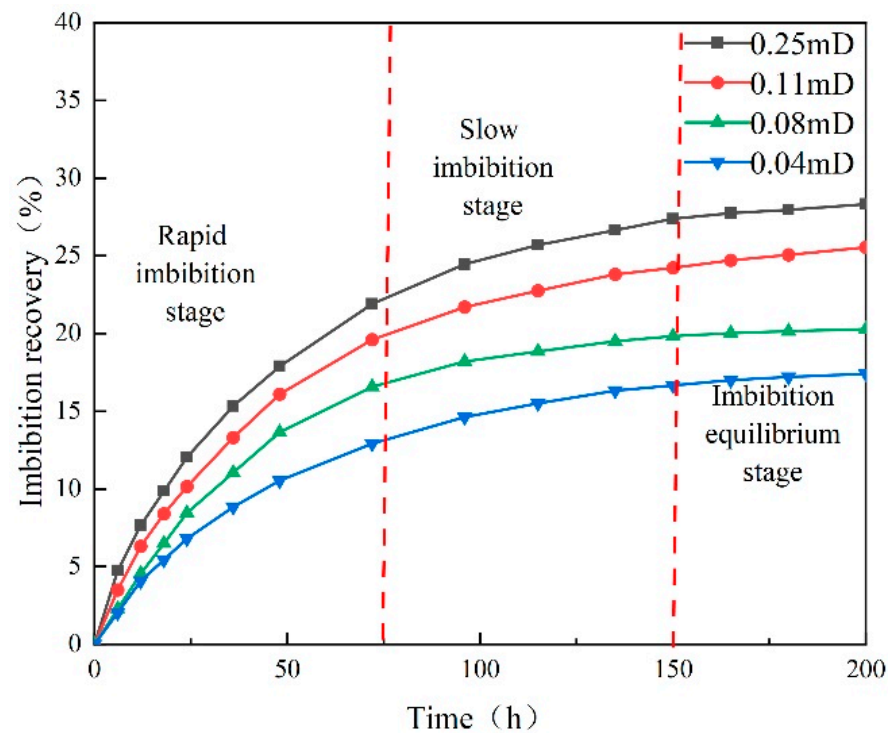


Figure 27. Imbibition recovery curves with different matrix permeabilities.

To investigate the imbibition effect of matrix permeability on CNI-A fracturing fluids further, we compared the pore mobilization of each pore with different matrix permeability. The different pore recoveries are shown in Figures 28–31. The experimental results indicate that the degree of pore mobilization is directly proportional to the matrix permeability, and the larger the permeability, the higher the degree of pore mobilization. In addition, in the imbibition process, due to the small radius of the micropores and the vigorous action of the capillary force, their contribution in the imbibition process is the largest, followed by the mesopores, and the macropores are relatively small. The results indicate that when the core permeability is less than 0.1 mD, the imbibition recovery increases rapidly with the increase of the core permeability. When the core permeability is more significant than 0.1 mD, the recovery increase rates slow down. The experimental results indicate that the imbibition recovery of CNI-A surfactant is between 15% and 30%, and CNI-A surfactant significantly improves the imbibition recovery. The main reasons can be attributed to two factors. Firstly, tight reservoirs exhibit a distinctive pore structure with an overall small pore throat radius, intensifying the effect of capillary forces and enhancing crude oil flow. Secondly, higher core permeability fosters better connectivity between the pore space and throat, reducing fluid seepage resistance.

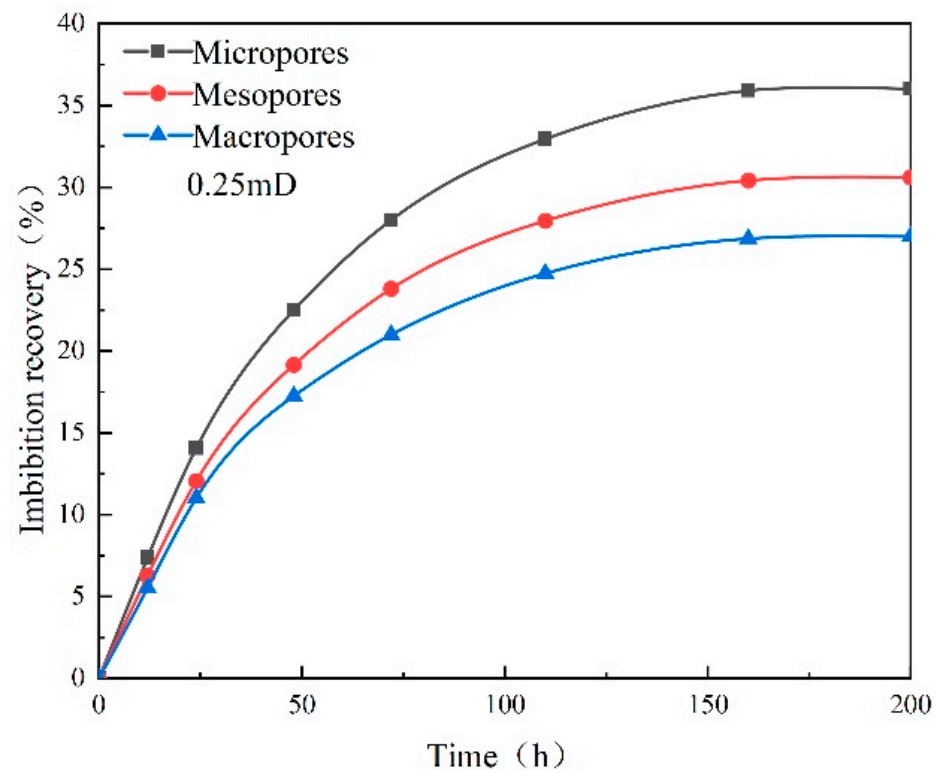


Figure 28. Matrix permeability of 0.25 mD different pore recovery.

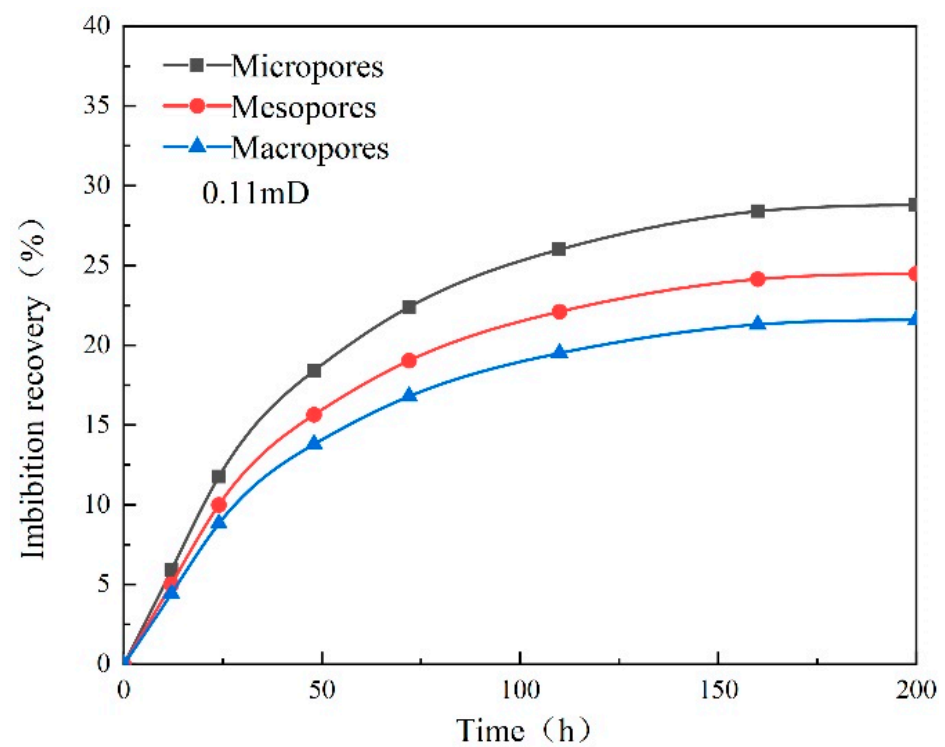


Figure 29. Matrix permeability of 0.11 mD different pore recovery.

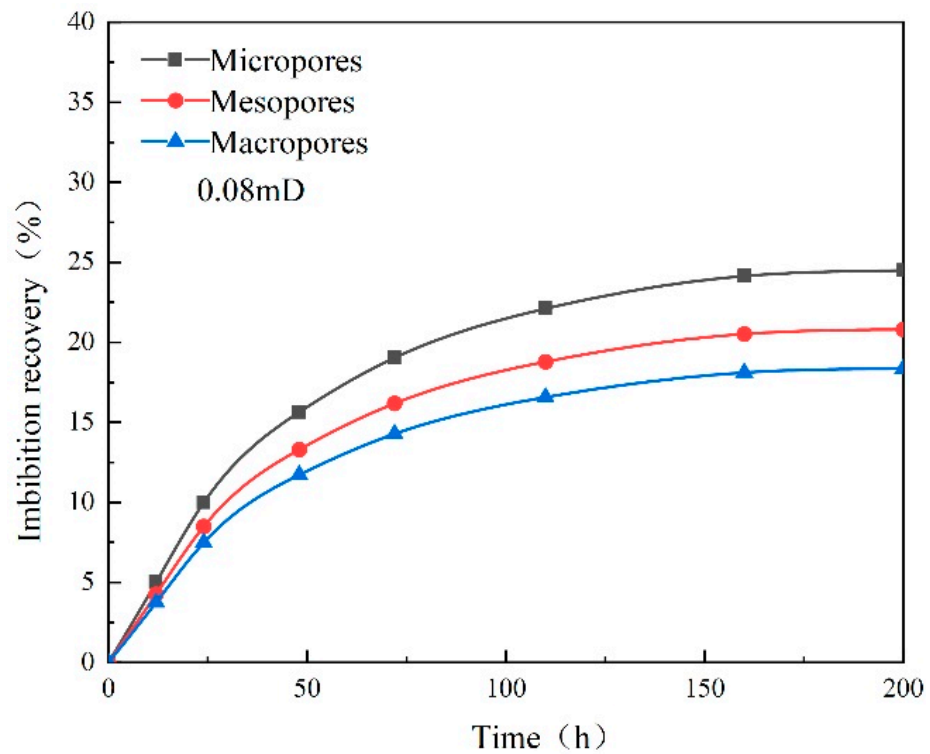


Figure 30. Matrix permeability of 0.08 mD different pore recovery.

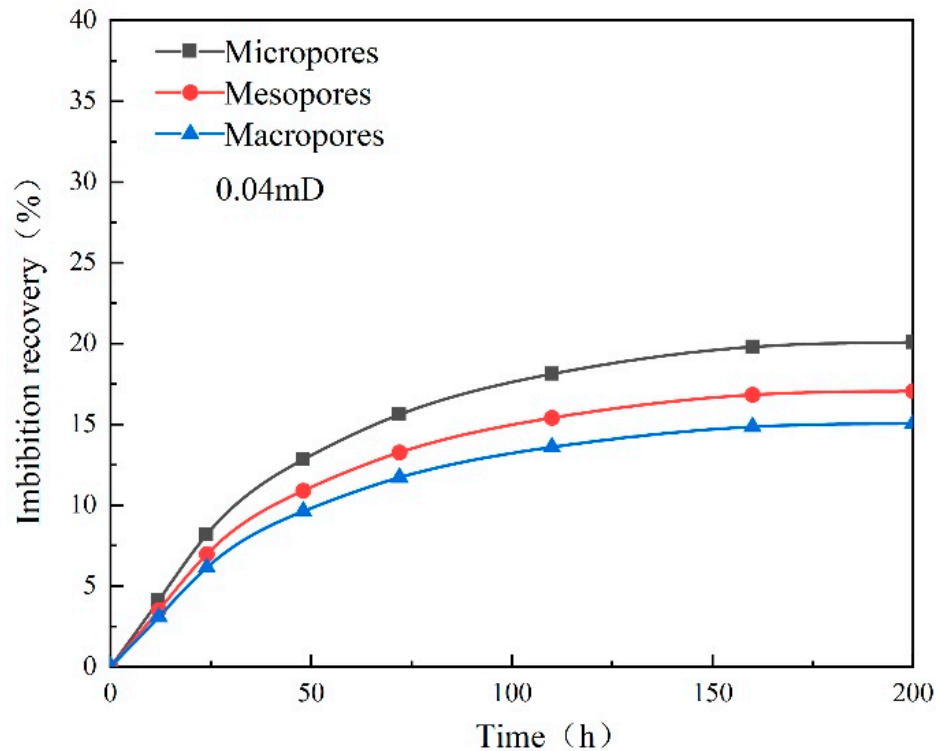


Figure 31. Matrix permeability of 0.04 mD different pore recovery.

Conversely, lower permeability corresponds to a smaller pore-throat radius, increasing complexity in pore-throat parameters, and enhanced heterogeneity. In such instances, although capillary force drives imbibition, the limited driving force makes it challenging for fluid to displace oil from porous media. This explains the lower recovery rates associated with low permeability. The CNI-A surfactant, known for its high fluidity, also acts

as a clay swelling inhibitor, enhancing fluid flow capacity. Its capillary pressure-driven penetration into deep reservoirs increases contact with crude oil, improving imbibition recovery. Additionally, CNI-A surfactant effectively reduces interfacial tension between fluids, altering rock interfacial properties and enhancing rock surface hydrophilicity, promoting the imbibition process. Moreover, elevated temperatures reduce fluid viscosity, expanding the imbibition sweep and maximizing ion exchange functionality for improved recovery. CNI fracturing fluid can change the wettability; the contact angle change before and after imbibition has been analyzed in the experimental part; and the contact becomes smaller after imbibition, which indicates that the fracturing fluid can change the wettability. Imbibition is the process of wettability replacing the non-wetted phase, and imbibition mainly occurs in hydrophilic reservoirs, and the more hydrophilic the rock is, the better the effect of imbibition is, so that changing the wettability can increase the recovery rate of imbibition. In terms of ion exchange: (1) the charge density of the rock surface is usually related to the temperature, and with the rise of temperature, the charge density of the rock surface may change; (2) the rise in temperature will increase the diffusion rate of dissolved ions, speeding up the reaction rate and making the rock surface of the ions adsorb and release more rapidly; (3) surfactants can reduce the surface tension of the oil phase, improving the properties of the interface between oil and water, which will influence the seepage and absorption process. In addition, the presence of a surfactant affects the charge distribution on the reservoir rock surface and influences the exchange rate. By forming complexes with ions, surfactants may affect the adsorption of ions. (4) This indicates that surfactants affect the pore structure of the reservoir, leading to changes in the channels and paths of ion diffusion in the pores and affecting ion exchange.

4. Conclusions

This paper used NMR to conduct imbibition experiments of fracturing fluids in tight reservoirs to investigate the effects of temperature, pressure, and matrix permeability on the imbibition effect. Based on the pore structure division, the contribution of each pore to the recovery was quantitatively analyzed, and the pore mobilization law in the process of imbibition was revealed. The main conclusions are as follows.

- (1) Imbibition recovery from CNI-A fracturing fluids in tight reservoirs ranges from 15% to 30%. During the imbibition process, the highest imbibition recoveries were obtained from micropores, and the smallest recoveries were obtained from macropores.
- (2) In the range of 0 MPa to 5 MPa, the pressure is positively correlated with imbibition recovery and pore mobilization. However, when the experimental pressure exceeds 5 MPa, increasing the pressure only changes the imbibition rate without further increasing the imbibition recovery.
- (3) As the temperature increases, the viscosity of crude oil decreases, the seepage capacity increases, and the degree of imbibition recovery and pore mobilization gradually increases.
- (4) In the scope of this paper, matrix permeability is positively correlated with imbibition recovery and pore mobilization. Changes in pore structure and connectivity can significantly improve the imbibition effect.

It can be learnt from this study that the imbibition of fracturing fluid can significantly improve the imbibition effect and increase the recovery of tight oil reservoirs. In addition, it is found that the temperature is positively correlated with the matrix permeability, so the reservoir permeability can be changed by hydraulic fracturing to improve the tight oil reservoir production. Meanwhile, pressure is positively correlated with imbibition recovery within a certain range, so it is recommended to adopt a reasonable time of well simmering to keep the pressure within a reasonable range, so as to efficiently play the role of imbibition replacement. From the analysis of the experimental conclusions, the study in this paper is mainly based on the fracturing fluid imbibition recovery rate in tight reservoirs and the influencing factors, and it has not yet been possible to carry out the study related to the distance of fracturing fluid imbibition. It is therefore suggested that a future experiment

can be carried out from the distance of fracturing fluid imbibition, to further analyze the impact of imbibition on the recovery of tight oil reservoirs.

Compared with the current experimental study of water imbibition at room temperature and pressure, this paper carries out imbibition experiments of fracturing fluid under high temperature and high pressure by using a nuclear magnetic resonance (NMR) experimental device, and clarifies the influence of fracturing fluid imbibition on the recovery rate of tight reservoirs, as well as clarifies the pore mobilization law in the process of imbibition, which can be used to provide a certain guidance for the development of tight reservoirs.

Author Contributions: Methodology, J.L.; Validation, Q.L.; Writing—original draft, X.Q., L.Z. and T.H.; Writing—review & editing, J.W.; Supervision, H.Y. All authors have read and agreed to the published version of the manuscript.

Funding: This research was funded by the National Natural Science Foundation of China (52074317) and Strategic Cooperation Technology Projects of CNPC and CUPB (ZLZX2020-02-04-04).

Data Availability Statement: Data are contained within the article.

Conflicts of Interest: Authors Jian Liu, Xuefeng Qu, Jiwei Wang and Qiang Liu was employed by the company PetroChina Changqing Oilfield Company. The remaining authors declare that the research was conducted in the absence of any commercial or financial relationships that could be construed as a potential conflict of interest. The authors declare that this study received funding from Strategic Cooperation Technology Projects of CNPC and CUPB. The funder was not involved in the study design, collection, analysis, interpretation of data, the writing of this article or the decision to submit it for publication.

Abbreviations

σ	Interfacial tension mN/m
ω	Angular velocity rad/s
R	radius μm
ρ	Density kg/m^3

References

1. Yang, K.; Wang, F.Y.; Zhao, J.Y. Experimental study of surfactant-enhanced spontaneous imbibition in fractured tight sandstone reservoirs: The effect of fracture distribution. *Pet. Sci.* **2023**, *20*, 380–381. [[CrossRef](#)]
2. Qi, S.C.; Yu, H.Y.; Han, X.B. Countercurrent imbibition in low-permeability porous media: Non-diffusive behavior and implications in tight oil recovery. *Pet. Sci.* **2023**, *20*, 322–336. [[CrossRef](#)]
3. Li, H.; Wang, C.; Li, B. Experimental Investigation on the Imbibition Behavior of Nanofluids in the Tight Oil and Gas Reservoir through the Application of Nuclear Magnetic Resonance Method. *Energies* **2023**, *16*, 454. [[CrossRef](#)]
4. Zhang, X.P.; Liu, Y.Q.; Liu, Y. Influencing Factors and Application of Spontaneous Imbibition of Fracturing Fluids in Tight Sandstone Gas Reservoir. *ACS Omega* **2022**, *7*, 38912–38922. [[CrossRef](#)]
5. Sun, Y.P.; Li, Q.J.; Chang, C. NMR-Based Shale Core Imbibition Performance Study. *Energies* **2022**, *15*, 6319. [[CrossRef](#)]
6. Pan, B.; Clarkson, C.R.; Younis, A. New methods to evaluate impacts of osmotic pressure and surfactant on fracturing fluid loss and effect of contact angle on spontaneous imbibition data scaling in unconventional reservoirs. *Fuel* **2022**, *328*, 125328–125338. [[CrossRef](#)]
7. Gong, R.D.; Wang, X.K.; Li, L. Lattice Boltzmann Modeling of Spontaneous Imbibition in Variable-Diameter Capillaries. *Energies* **2022**, *15*, 4254. [[CrossRef](#)]
8. Lyu, Q.; Wang, K.; Hu, C. Effects of supercritical CO₂/water imbibition under dynamic pressures on shale mechanics and acoustic emission characteristics. *Fuel* **2022**, *321*, 124087–124097. [[CrossRef](#)]
9. Zhang, L.L.; Wang, K.L.; An, H.M. Spontaneous Imbibition of Capillaries under the End Effect and Wetting Hysteresis. *ACS Omega* **2022**, *7*, 4363–4371. [[CrossRef](#)]
10. Yue, M.; Li, B.B.; Chen, Q. Experimental Investigation on the Effect of Pore Size on Spontaneous Imbibition Recovery in Oil-Wet Reservoirs. *Geofluids* **2022**, *2022*, 4319832. [[CrossRef](#)]
11. Wang, K.; Jiang, B.B.; Ye, K.R. Spontaneous imbibition model for micro–nano–scale pores in shale gas reservoirs considering gas–water interaction. *J. Pet. Sci. Eng.* **2022**, *209*, 109893–109899. [[CrossRef](#)]
12. Xu, R.Z.; Yang, S.L.; Xiao, Z.P. Quantitatively study on imbibition of fracturing fluid in tight sandstone reservoir under high temperature and high pressure based on NMR technology. *J. Pet. Sci. Eng.* **2022**, *208*, 109623–109633. [[CrossRef](#)]

13. Dou, L.; Xiao, Y.; Gao, H. The study of enhanced displacement efficiency in tight sandstone from the combination of spontaneous and dynamic imbibition. *J. Pet. Sci. Eng.* **2021**, *199*, 108327–108337. [[CrossRef](#)]
14. Zhu, D.; Li, B.F.; Li, H.F. Effects of low-salinity water on the interface characteristics and imbibition process. *J. Pet. Sci. Eng.* **2022**, *208*, 109564–109569. [[CrossRef](#)]
15. Xu, D.R.; Li, Z.; Bai, B.J. A systematic research on spontaneous imbibition of surfactant solutions for low permeability sandstone reservoirs. *J. Pet. Sci. Eng.* **2021**, *206*, 109003–109010. [[CrossRef](#)]
16. Zhang, P.F.; Lu, S.F.; Li, J.Q. Evaluating micro-distribution of adsorbed and free oil in a lacustrine shale using nuclear magnetic resonance: A theoretical and experimental study. *J. Pet. Sci. Eng.* **2022**, *212*, 110208–110218. [[CrossRef](#)]
17. Wang, X.J.; Wang, M.; Li, Y. Shale pore connectivity and influencing factors based on spontaneous imbibition combined with a nuclear magnetic resonance experiment. *Mar. Pet. Geol.* **2021**, *132*, 105239–105249. [[CrossRef](#)]
18. Liu, D.K.; Ren, D.Z.; Du, K. Impacts of mineral composition and pore structure on spontaneous imbibition in tight sandstone. *J. Pet. Sci. Eng.* **2021**, *201*, 108397–108407. [[CrossRef](#)]
19. Arab, D.; Bryant, S.L.; Tortor, O. Water flooding of sandstone oil reservoirs: Underlying mechanisms in imbibition vs. drainage displacement. *J. Pet. Sci. Eng.* **2022**, *213*, 110379–110389. [[CrossRef](#)]
20. Wang, C.; Gao, H.; Gao, Y. Influence of Pressure on Spontaneous Imbibition in Tight Sandstone Reservoirs. *Energy Fuels* **2020**, *34*, 9275–9282. [[CrossRef](#)]
21. Ding, Y.; Liu, X.J.; Liang, L.X. Experimental and model analysis on shale spontaneous imbibition and its influence factors. *J. Nat. Gas Sci. Eng.* **2022**, *99*, 104462–104472. [[CrossRef](#)]
22. Sukee, A.; Nunta, T.K.; Haruna, M.J.A. Influence of sequential changes in the crude oil-water interfacial tension on spontaneous imbibition in oil-wet sandstone. *J. Pet. Sci. Eng.* **2022**, *210*, 110032–110043. [[CrossRef](#)]
23. Xia, Y.; Tian, Z.; Xu, S. Effects of microstructural and petrophysical properties on spontaneous imbibition in tight sandstone reservoirs. *J. Nat. Gas Sci. Eng.* **2021**, *96*, 104225–104235. [[CrossRef](#)]
24. Zheng, H.; Liao, R.Q.; Cheng, N. Microscopic mechanism of fracturing fluid imbibition in stimulated tight oil reservoir. *J. Pet. Sci. Eng.* **2021**, *202*, 108533–108543. [[CrossRef](#)]
25. Yu, H.; Song, J.; Chen, Z. Numerical study on natural gas injection with allied in-situ injection and production for improving shale oil recovery. *Fuel* **2022**, *318*, 123586–123596. [[CrossRef](#)]
26. Yu, H.; Fu, W.; Zhang, Y. Experimental study on EOR performance of CO₂-based flooding methods on tight oil. *Fuel* **2021**, *290*, 119988–119998. [[CrossRef](#)]
27. Yu, H.; Rui, Z.; Chen, Z. Feasibility study of improved unconventional reservoir performance with carbonated water and surfactant. *Energy* **2019**, *182*, 135–147. [[CrossRef](#)]
28. Li, M.; Yang, H.; Lu, H. Investigation into the Classification of Tight Sandstone Reservoirs via Imbibition Characteristics. *Energies* **2018**, *11*, 2619. [[CrossRef](#)]
29. Li, M.M.; Li, Q.; Bi, G. A Two-Phase Flow Model for Pressure Transient Analysis of Water Injection Well considering Water Imbibition in Natural Fractured Reservoirs. *Math. Probl. Eng.* **2018**, *9*, 2313–2323. [[CrossRef](#)]
30. Lai, F.P.; Li, Z.P.; Zhang, T.T. Characteristics of microscopic pore structure and its influence on spontaneous imbibition of tight gas reservoir in the Ordos Basin, China. *J. Pet. Sci. Eng.* **2018**, *172*, 23–31. [[CrossRef](#)]
31. Lyu, C.; Wang, Q.; Ning, Z. Investigation on the Application of NMR to Spontaneous Imbibition Recovery of Tight Sandstones: An Experimental Study. *Energies* **2018**, *11*, 2359. [[CrossRef](#)]
32. Wang, X.; Peng, X.; Zhang, S.; Du, Z.; Zeng, F. Characteristics of oil distributions in forced and spontaneous imbibition of tight oil reservoir. *Fuel* **2018**, *224*, 280–288. [[CrossRef](#)]
33. Li, J.; Yu, W.; Guerra, D. Modeling wettability alteration effect on well performance in Permian basin with complex fracture networks. *Fuel* **2018**, *224*, 740–751. [[CrossRef](#)]
34. Hou, B.F.; Wang, Y.F.; Huang, Y. Imbibition of Water by Oil-Wet Sandstone Cores Using Different Surfactants. *J. Dispers. Sci. Technol.* **2015**, *36*, 1264–1273. [[CrossRef](#)]
35. Qu, M.; Liang, T.; Xiao, L. Mechanism study of spontaneous imbibition with lower-phase nano-emulsion in tight reservoirs. *J. Pet. Sci. Eng.* **2021**, *211*, 110220. [[CrossRef](#)]
36. Tian, W.; Wu, K.; Gao, Y. A critical review of enhanced oil recovery by imbibition: Theory and practice. *Energy Fuels* **2021**, *35*, 5643–5670. [[CrossRef](#)]
37. Lin, W.; Xiong, S.; Liu, Y. Spontaneous imbibition in tight porous media with different wettability: Pore-scale simulation. *Phys. Fluids* **2021**, *33*, 3565–3587. [[CrossRef](#)]
38. Qin, C.Z.; Wang, X.; Zhang, H. Numerical studies of spontaneous imbibition in porous media: Model development and pore-scale perspectives. *J. Pet. Sci. Eng.* **2022**, *218*, 110961–110971. [[CrossRef](#)]
39. Li, S.; Liu, H.; Wu, R. Prediction of spontaneous imbibition with gravity in porous media micromodels. *J. Fluid Mech.* **2022**, *952*, A9. [[CrossRef](#)]
40. Cao, B.; Lu, X.; Xie, K. The pore-scale mechanisms of surfactant-assisted spontaneous and forced imbibition in water-wet tight oil reservoirs. *J. Pet. Sci. Eng.* **2022**, *213*, 110371–110381. [[CrossRef](#)]
41. Yang, Y.; Wang, S.; Feng, Q. Imbibition Mechanisms of Fracturing Fluid in Shale Oil Formation: A Review from the Multiscale Perspective. *Energy Fuels* **2023**, *37*, 9822–9840. [[CrossRef](#)]

42. Ren, D.; Ma, L.; Liu, D. Control mechanism and parameter simulation of oil-water properties on spontaneous imbibition efficiency of tight sandstone reservoir. *Front. Phys.* **2022**, *10*, 829763–829773. [[CrossRef](#)]
43. Liu, Y.; Rui, Z. A storage-driven CO₂ EOR for a net-zero emission target. *Engineering* **2022**, *18*, 79–87. [[CrossRef](#)]
44. Pandey, A.; Qamar, S.F.; Das, S.; Basu, S.; Kesarwani, H.; Saxena, A.; Sharma, S.; Sarkar, J. Advanced multi-wall carbon nanotube-optimized surfactant-polymer flooding for enhanced oil recovery. *Fuel* **2024**, *355*, 129463–129469. [[CrossRef](#)]
45. Pandey, A.; Roy, V.; Kesarwani, H.; Sharma, S.; Saxena, A. Evaluation of Silicon Carbide Nanoparticles as an Additive to Minimize Surfactant Loss during Chemical Flooding. *Chem. Sel.* **2022**, *7*, e202104294. [[CrossRef](#)]
46. Nicasy RJ, K.; Barquero, A.; Huinink, H.P.; Erich, S.J.F.; Adan, O.C.G.; Tomozeiu, N.; Mansouri, H.; Scheerder, J. Increasing particle concentration enhances particle penetration depth but slows down liquid imbibition in thin fibrous filters. *Colloids Surf. A Physicochem. Eng. Asp.* **2024**, *684*, 133146. [[CrossRef](#)]
47. Bloch, P.Y.; Olejnik, K.; Bloch, J.F.; Bloch, A.; Hammond, J.; Brissaud, D. Time Scales of Spontaneous Imbibition into Porous Material: From Classic Models to Papers Applications. *Bio Resour.* **2024**, *19*, 345–365. [[CrossRef](#)]

Disclaimer/Publisher’s Note: The statements, opinions and data contained in all publications are solely those of the individual author(s) and contributor(s) and not of MDPI and/or the editor(s). MDPI and/or the editor(s) disclaim responsibility for any injury to people or property resulting from any ideas, methods, instructions or products referred to in the content.